# Graphene oxide incorporated polyether sulfone nanocomposite antifouling ultrafiltration membranes with enhanced hydrophilicity

Materials Research Express

PAPER

# Graphene oxide incorporated polyether sulfone nanocomposite antifouling ultrafiltration membranes with enhanced hydrophilicity

**Amber Salim**[1], **Muhammad Asad Abbas**[1], **Imran Ahmad Khan**[1], **Muhammad Zafar Khan**[1], **Farhan Javaid**[1], **Shehla Mushtaq**[2], **Mehwish Batool**[3], **Muhammad Yasir**[4], **Asim Laeeq Khan**[3], **Asad U Khan**[1], **Kashif Mairaj Deen**[5,*] **and Nasir M Ahmad**[1,*]

[1] School of Chemical and Materials Engineering (SCME), National University of Sciences and Technology (NUST), H-12, Islamabad, Pakistan
[2] School of Natural Sciences, National University of Sciences and Technology (NUST), H-12, Islamabad, Pakistan
[3] Department of Chemical Engineering, COMSATS University Islamabad, Lahore Campus, Lahore, Pakistan
[4] Centre of Polymer Systems, University Institute, Tomas Bata University in Zlín, Třída Tomáše Bati 5678, 760 01Zlín, Czech Republic
[5] Department of Materials Engineering, The University of British Columbia, Vancouver, V6T 1Z4, BC, Canada
[*] Authors to whom any correspondence should be addressed.

**E-mail:** kashifmairaj.deen@ubc.ca **and** nasir.ahmad@scme.nust.edu.pk

**Keywords:** membranes, fouling, nanocomposites, antibacterial

OPEN ACCESS

RECEIVED
19 May 2022

REVISED
10 July 2022

ACCEPTED FOR PUBLICATION
15 July 2022

PUBLISHED
26 July 2022



## Abstract

In this study, the polyether sulfone (PES) based membranes containing various concentrations of graphene oxide (GO), polyvinylpyrrolidone (PVP), and polyethylene glycol (PEG) were synthesized via the phase immersion method. This study aims to evaluate the effect of GO addition on the structural properties and performance of the membranes. The membranes were analyzed by x-ray diffraction (XRD), scanning electron microscopy (SEM), and Fourier transforms infrared spectroscopy (FTIR). The FTIR-ATR spectra indicated the presence of hydroxyl and carboxylic acid groups on the surface of GO-incorporated membranes, which improved their dispersion in the polymeric matrix and hydrophilicity. The SEM analysis of the GO-containing PES membranes confirmed the formation of a well-defined finger-like porous structure presenting adequate water flux (95 $l.m^{-2}.h^{-1}$) and salt rejection (72%) compared to the pristine PES membranes (46 $l.m^{-2}.h^{-1}$ and ~35%, respectively). In addition, the significantly large wettability and considerably improved antibacterial characteristic (against *S. aureus* and *E. coli strains*) of the GO-PES membranes are considered impressive features.

## 1. Introduction

Wastewater is a potential resource that can be reused after treatment to overcome not only water pollution but also to meet the ever-increasing demand for potable water supplies for the global population, industrial sectors, and expanding economies (Boretti and Rosa 2019). However, water purification is an energy-intensive and expensive process (Gontarek-Castro *et al* 2021). There is a dire need to develop novel approaches for water purification that use less energy, are cost-effective, and most importantly, are environmentally friendly (Goh *et al* 2020). The use of membranes in the treatment of wastewater is well justifiable as these offer several advantages over other processes owing to their high surface area, appreciable separation efficiency, low chemical sludge effluent, and easy maintenance (Du *et al* 2009).

Polymers offer a wide diversity of structures and properties. Almost all organic membranes explored so far are mainly made up of polymeric materials (Du *et al* 2009). Despite being low cost, the main drawback of polymeric membranes is the innate hydrophobicity that enhances their fouling tendency, having a shorter lifetime, high operation cost, low filtration efficiency, and are only suitable for customized application (Mansouri *et al* 2010). The buildup of inorganics, organics, proteins, microbial species, and microorganisms on the membrane surface is known as fouling (Rana and Matsuura 2010, Arif *et al* 2019). Consequently, the synthesis of novel functionalities in polymeric membranes is focused on improving the next generation of polymeric membrane technology (Ulbricht 2006). Generally, no polymeric membrane simultaneously

manifests mechanical strength, pH/oxidation resistance, thermal and chemical stability. Hence, significant research is conducted towards enhancing pollution resistance, permeation flux, working pressure stability, and longevity of the membranes (Ngo *et al* 2016). As most of the anti-fouling agents are hydrophobic, one effective strategy to reduce the fouling issues could be making the polymeric membranes hydrophilic (Elimelech 2004). Wastewater treatment involves different membranes, based on their pore size regimes: microfiltration, nanofiltration, ultrafiltration, reverse osmosis, and particle filtration membranes (Choudhury *et al* 2018). Membranes are categorized based on the similarity of their two faces or porosity difference (Choudhury *et al* 2018). For instance, membranes are categorized as asymmetric when their two faces differ in porosity or symmetric when the two faces have similar porosity (Jeon *et al* 2016). Symmetrical membranes being resistant to fluid flow possess slower flow rates than asymmetrical membranes of similar retentivity (Esfahani *et al* 2019). On the other hand, a phase inversion method is used to prepare asymmetrical membranes (Esfahani *et al* 2019). This method consists of a solution comprising solvent and polymer that is submerged in a non-solvent coagulation bath (Esfahani *et al* 2019). Diffusion of non-solvent and solvent in the casting solution undergoes a phase transition, resulting in the formation of the polymeric membrane (Qadir *et al* 2017). Many factors i.e. interactions between polymer-solvent, solvent-nonsolvent, and coagulation bath temperature significantly influence the membrane fabrication process (Qadir *et al* 2017).

Due to their high glass transition temperature, excellent selectivity, high chemical resistance, better mechanical stability, and improved permeability, polyethersulfone (PES) and polysulfone (PSU) are the commonly used polymers to fabricate reverse osmosis, nanofiltration, and ultrafiltration membranes (Zhao *et al* 2013). A study shows that PES membranes added with Polyvinyl pyrrolidone (PVP) have increased water adsorption, water flux, and decreased water contact angle compared to pure PES membranes (Guo *et al* 2020). Moreover, it was found that PES membranes with the best mechanical properties (in terms of elongation and tensile strength) are obtained by adding 1 wt% PVP to the casting film (Said *et al* 2018). Similarly, another study found that the addition of 10 wt% PVP concentration decreased the contact angle by 16%. The impact of PVP on membrane formation was also investigated by (Chou *et al* 2005). Their results show that PVP addition to the ternary system restrains macro voids formation in the sub-layer, which is desired in high pressure-driven operation to increase the strength of the membrane while lowering its chances of collapse (Chou *et al* 2005). Similarly, another set of researchers discovered that adding a little amount of PVP to casting film increases the permeability of PES-based ultrafiltration membranes without significantly affecting selectivity (Ying *et al* 2017). The surface hydrophilicity of PES membranes can also be improved by adding different nanoparticles like $TiO_2$, ZnO, Ag, graphene oxide (GO), CNT, nitrates, carboxylates, and sulfonation to PES (Kim *et al* 2014, Lu le *et al* 2015). It can also include the grafting of various functional polymers on the PES backbone. Furthermore, interfacial polymerization and various methods of grafting polymerization such as UV-based grafting, atom transfer radical polymerization (ATRP), ozone, redox, plasma, and thermal treatments could potentially modify the PES backbone (Shahkaramipour *et al* 2017). Besides, GO has also been used as a membrane filler and resulted in a favorable product for potential application in non-aqueous and aqueous industrial separation processes (Shahkaramipour *et al* 2017). In another study, GO embedded PES matrix not only registered a large flux but also presented high fouling resistance (Ji *et al* 2017) (Yin and Deng 2015). Similarly, GO-modified PES membranes attained high antifouling and salt rejection characteristics. Wang *et al* 2019, reported the fabrication of PES-GO membranes via the electrical field-assisted phase inversion method, which showed a significant improvement in the antifouling characteristics. In another study (Alammar *et al* 2020), polybenzimidazole (PBI)-GO membranes showed excellent antifouling and water treatment capabilities. Moreover, GO coating on PES membranes has filtration capacity against arsenic ions and methylene blue dye from an aqueous solution as reported elsewhere (Park *et al* 2019).

In this study, the effect of varying amounts of PEG, PVP, and GO as nano-filler in the PES matrix membranes has been investigated. For instance, the addition of these species and their impact on the pore size, pore distribution, and water permeability have been measured. The membranes exhibiting high efficiency of water permeability were further scrutinized by measuring their surface wettability and water uptake capacity. Salt rejection capability and antibacterial performance of the GO-based nano-fillers PES membrane have also been estimated to evaluate their filtration and antifouling behavior.

## 2. Materials and methods

### 2.1. Chemicals

In this research work, analytical grade chemicals were used as received without further purification. PES (M.W. 58,000 g $mole^{-1}$) and N-methyl-2-pyrrolidone (NMP) solvent were purchased from Ultrasone and Sigma-Aldrich (Germany), respectively. PVP (M.W. 40,000 g $mole^{-1}$), and GO were purchased from Merck and Sigma Aldrich, Germany.

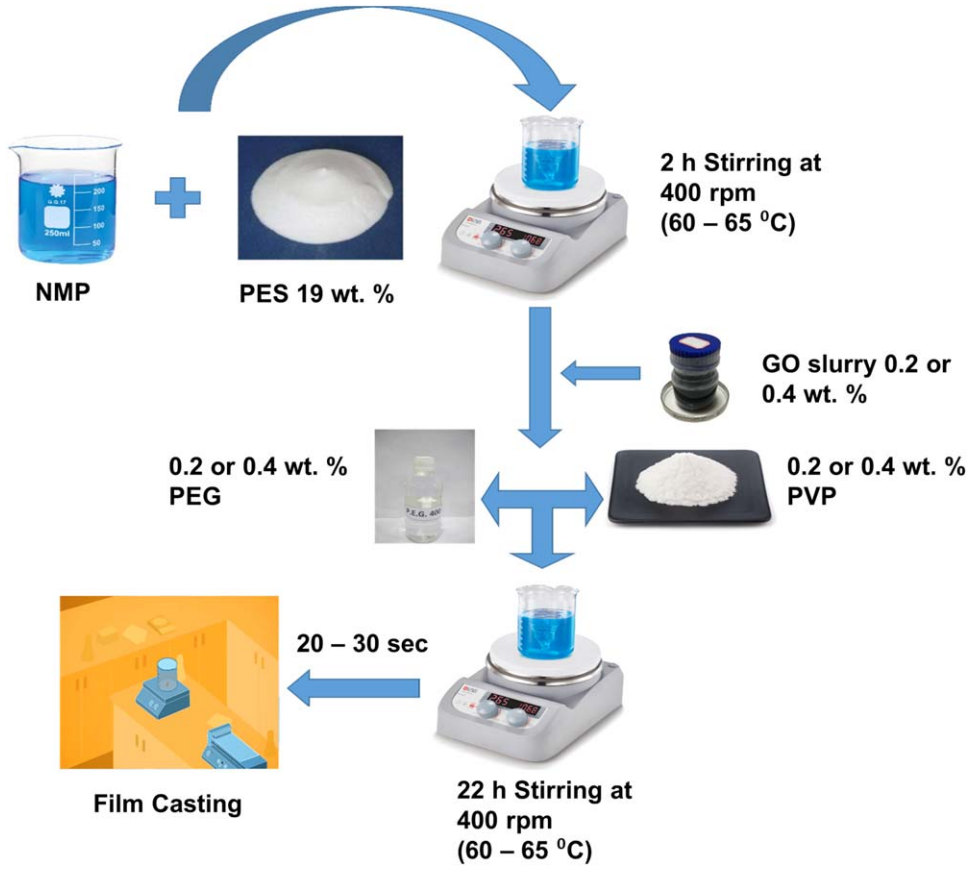


**Figure 1.** A schematic representation of the membrane synthesis process.

### 2.2. Preparation of membranes

The membranes were prepared by using various solutions of polymers consisting of about 19 wt% PES as a matrix phase polymer. Dense membranes were fabricated using asymmetric PES-based flat sheets containing GO by phase inversion and immersion precipitation methods. A PES polymer (19 wt%), PVP (1.0 wt%) and various amounts of GO were dissolved in the NMP solvent. As reported elsewhere (Kiran *et al* 2016, Bhatti *et al* 2018), a high concentration of GO could increase aggregation, decrease porosity, pore size and wettability. Based on these reasons, a low GO concentration of 0.2 and 0.4 wt% was added to the PES during the membrane synthesis process. A non-solvent phase inversion method was used to prepare membranes having various compositions. The schematic diagram of the membrane synthesis process is shown in figure 1. Briefly, the casting solutions were synthesized by adding different amounts of polymer (PES). Pore former and solvent (NMP) were added together in a media bottle under continuous stirring at 400 rpm for 24 h (at room temperature ~23 °C) to make a homogenous solution. The process continued until the polymer and all other related constituents were thoroughly homogenized. To remove the trapped air bubbles, sonication was carried out for about 15–20 min at ~23 °C. The prepared homogenous solutions were uniformly cast by using an automatic film applicator (Filmography, Elcometer) having a casting speed of about 2 cm.s$^{-1}$ by using a 250 $\mu$m thick casting knife. The films were prepared onto a non-warm polyethylene/polypropylene support firmly affixed to a glass plate. The casting was performed in a controlled environment i.e. at ~23 °C and 20% relative humidity. The resulting fabricated membranes were immersed in a mixture of water and isopropanol mixture (70/30) for 19 h and kept in glycerol for 4 h to preserve the pore structure. During the casting process, the temperature was maintained constant at 18 °C $\pm$ 1 °C. To permit polymer coagulation, the glass plate was dipped in the water bath after casting at ambient temperature. The prepared membranes were washed repeatedly using distilled water to remove any remaining solvent before storage in ultra-pure water for further use. Before testing, the cast membranes were kept in deionized water for 24 h and dried by sandwiching in the filter papers. Table 1 shows casting solution compositions with relative membrane designations as used in this study. Three samples of each membrane were prepared and analyzed separately to estimate standard deviation and to ensure reproducibility in the results.

**Table 1.** Casting solution compositions of membrane samples.

| Membrane designation | PES (%) | PEG (%) | PVP (%) | GO (%) |
|---|---|---|---|---|
| PPE2 | 19 | 0.2 | — | — |
| PPE4 | 19 | 0.4 | — | — |
| PPV2 | 19 | — | 0.2 | — |
| PPV4 | 19 | — | 0.4 | — |
| PEPVGO2 | 19 | 0.2 | 0.2 | 0.2 |
| PEPVGO4 | 19 | 0.4 | 0.4 | 0.4 |

### 2.3. Membrane characterization

FTIR-ATR analysis of the as-prepared membranes was carried out to determine chemical composition. The FTIR-ATR spectra were obtained by scanning the membrane samples (0.25 × 0.25 $cm^2$) between 400–4000 $cm^{-1}$ wavenumbers with a resolution of about 2 $cm^{-1}$ by using an FTIR Spectrophotometer Model: ALPHA II. The crystal structure of the GO was characterized by x-ray diffraction within the 5°–50° 2$\theta$ range. The XRD pattern of the membrane samples having an area of 1 $cm^2$ was obtained by using a STOE $\theta$–$\theta$ diffractometer. The surface morphology and cross-sectional structure of the membranes were examined in a scanning electron microscope (SEM) (JEOL). Membrane samples of 0.25 × 0.25 $cm^2$ in size were mounted on the steel stubs before gold-sputtering before analysis to avoid the surface charging effects.

Owing to the non-contacting measuring principle of optical profilometry, the surface roughness of the membranes was measured without affecting their surface structure. Results indicate that scanning by using glass plates is also possible, but with certain limitations. However, under certain conditions, proper measurements can also be performed. The sample dimensions were 0.25 × 0.25 $cm^2$. A sessile drop method (A Fibro DAT 1100, Sweden) was applied to estimate the surface wettability of the membrane by measuring the contact angle of deionized (DI) water under ambient conditions. All membrane samples were completely dried before testing. The device is provided with a high-definition camera used to monitor the drop profile of lateral images as a function of time. Approximately 4 $\mu$l DI water was dropped on the surface of the dry membrane from a mini syringe at room temperature. To ensure reproducibility, all membrane samples were tested at least 6 times for contact angle measurements. To calculate the water uptake capacity, the membrane samples were soaked in DI water for 24 h. Briefly, the weight of the membrane samples before and after soaking in water was measured to calculate the water uptake capacity by using equation (1).

$$Water\ Uptake\ (\%) = \frac{W_{wet} - W_{dry}}{W_{wet}} \times 100 \tag{1}$$

The porosity of the membrane samples ($s$) was assessed by using a stepwise procedure. Briefly, the initial weight ($W_{dry}$) of the membranes was measured membranes after overnight drying in a vacuum oven at 40 °C. These membrane samples were soaked in DI water for 24 h to measure the weight of the wet membranes ($W_{wet}$). To estimate the quantity of the adsorbed water, the wet membrane samples were dried again in a vacuum oven at 40 °C for 24 h to remove all the absorbed water. and weighed again to measure the quantity of the adsorbed water. All measurements were done in triplicate to ensure reproducibility in the results. The gravimetric method was used to calculate '$s$' by using equation (2). Where, 'A', 't' and 'd' are the geometrical surface area, time and density of the membrane samples.

$$s = \frac{W_{wet} - W_{dry}}{A \times t \times d} \tag{2}$$

The volume of a fluid passing through a unit area of the membrane per unit time is defined as Permeation flux (J). The 'J' of the prepared membrane samples was determined by using a vacuum filtration assembly. Pure distilled water (10 ml) was passed through each membrane having an exposed surface area of 0.025 $m^2$. In this assembly, a vacuum pressure of about 60 cm of mercury was maintained and the time taken by 10 ml of water to pass through the membrane sample was recorded. The permeation flux of the membrane samples was determined by using equation (3).

$$Q = \frac{J}{AT} \tag{3}$$

Where 'J' denotes permeate flux (l $m^{-2}h^{-1}$), 'Q indicates the volume of the permeated water through the membrane samples (10 ml). 'A' is the effective surface area of the membrane and is the time taken for the nano-filtration (in hours) of the known volume of distilled water. To ensure reproducibility, the permeation flux tests were conducted in triplicate for each membrane sample. The salt (NaCl) rejection ability of the membrane samples was estimated from their nano-filtration capability. The salt rejection measurements were carried out in

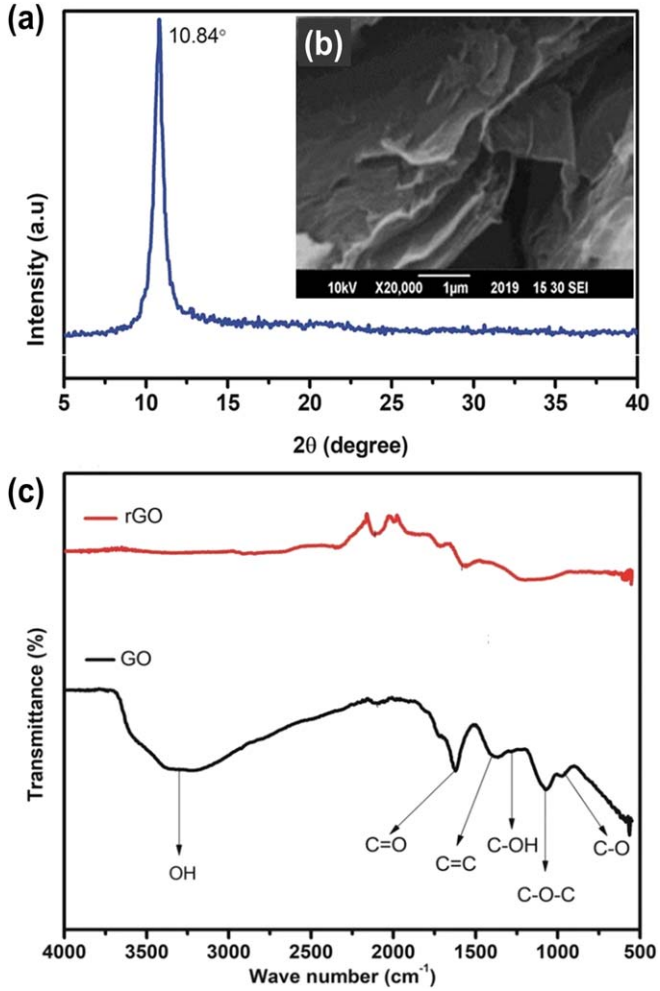


**Figure 2.** Characterization of the GO used in the synthesis of GO-PES membranes (a) XRD pattern, (b) SEM image, and (c) FTIR spectra of GO in comparison with rGO.

a dead-end nano-filtration cell containing 1000 ppm of NaCl at a pressure of 6 bar maintained. The duration of the salt rejection test was selected to be 1 h in addition to the initial 30 min stabilization at low pressure to homogenize the feed salt concentration within the membrane samples.

The antimicrobial susceptibility tests were carried out on Muller–Hinton (MH) agar plates. *S. aureus* and *E. coli* were stored in the MH Broth at 37 °C for 24 h before stirring at 150 rpm at 4 °C with the addition of 30% (v/v) glycerol solution. The resultant bacteria-containing suspension was further diluted to about 106–107 CFU $ml^{-1}$ with the addition of an MH medium.

During the disk diffusion test (Kirby–Bauer test), the *E. coli* and *S. aureus* strains were first introduced onto the MH agar plates with the help of cotton swabs from the prepared suspensions having 106–107 CFU $ml^{-1}$ initial concentration. Also, the GO paper disks of identical size were placed in the center of each Petri dish. After 24 h of incubation at 37 °C, the proliferation of the bacterial colonies was examined and the inhibition zone diameter was calculated.

## 3. Results and discussion

### 3.1. Characterization of the GO

Figure 2 shows the XRD, SEM, and FTIR analyses of the GO. A typical diffraction peak originating at 10.84° validated the characteristics (001) carbon peak. The SEM image of the GO also showed the stacked layered structure of graphene nanoplatelets as shown in figure 2(b). The FTIR spectrum of the GO was also obtained and compared with the reduced GO (rGO). The broad peak originated at 3390 $cm^{-1}$ corresponded to the OH group possibly associated with the $H_2O$ adsorption. However, no peak associated with the OH was observed in the case of rGO as shown in figure 2(c). The presence of carboxylic and carbonyl functional groups on the surface of GO was evident from the sharp peaks observed at 1720 and 1632 $cm^{-1}$. In addition to these, the existence of other

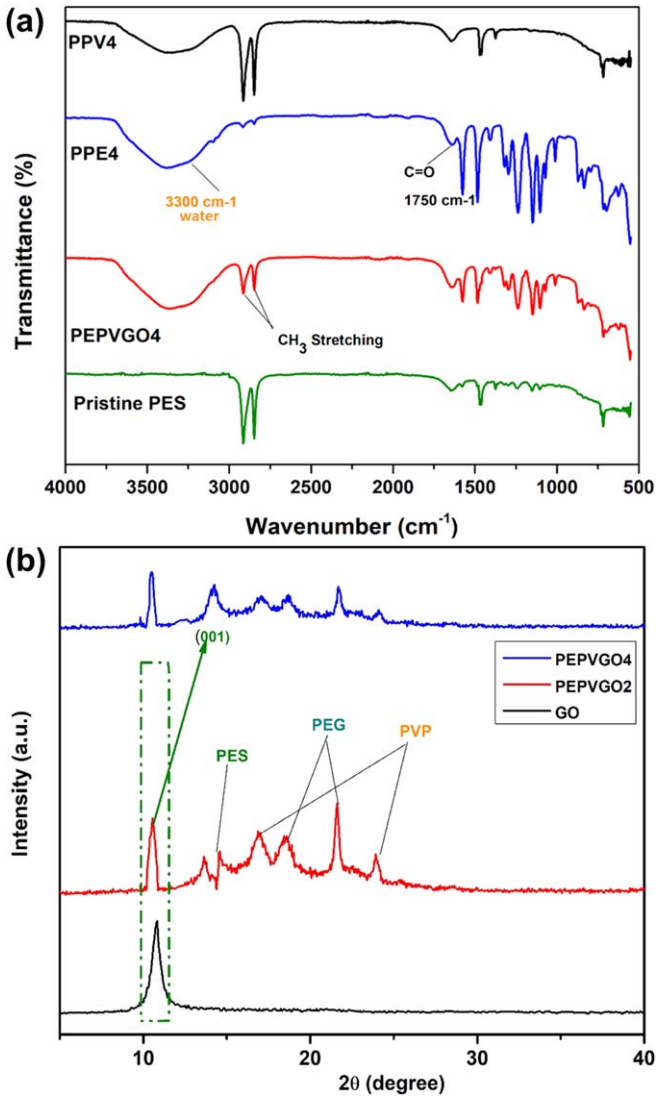


**Figure 3.** (a) FTIR spectra of the pristine and modified PES membrane samples obtained by the addition of various additives (**b**) XRD Pattern of the GO, PEPVGO2, and PEPVGO4 membrane samples.

functional groups (i.e. C=C, C–O–C, and C–O) also indicated the improved dispersion of the GO nanoplatelets in the PES, which ensures its homogenous distribution in the membranes.

### 3.2. Structural characterization of the synthetic membrane samples

The effect of GO addition on the chemical composition of the membrane was determined by ATR-FTIR analysis. The membrane samples were produced by varying the concentration of various additives in the PES matrix as discussed in section 2.2 and table 1. Figure 3(a) shows the ATR-FTIR spectra of the pristine and other versions of the membrane samples.

The peaks originating at 2600–2800 corresponding to C–H bond stretching vibrations were evident in all membrane samples (Abbas *et al* 2020) except in the PPE4 sample. The PPE4 membrane sample presented relatively depressed peaks associated with the stretching of C–H bonds. The peak signatures at ~1370 and 1467 $cm^{-1}$ indicated the symmetric and asymmetric stretching vibrations of the S=O bond, respectively (Batool *et al* 2021). In the case of PEPVGO4, PPE4 and PPV4, the broad peak that appeared at 3390 $cm^{-1}$ represented the presence of hydroxyl groups owing to the addition of PEG, PVP, and GO in the PES matrix. The characteristic peaks of the GO originated at 1094, 1150, and 1258 $cm^{-1}$ highlighting the presence of stretched C–O–C, COH, and C=C bonds of the aromatic ring, respectively (Qian *et al* 2018). In PEPVGO4, the addition of 0.4% GO registered very small amplitude C–O–C, COH, and C=C peaks.

The diffraction patterns of the GO-containing PES membrane are shown in figure 3(b). Pristine GO displayed a dominant peak at $2\theta = 10.8^{\circ}$ associated with the graphite oxide (0 0 1) (Gontarek-Castro *et al* 2021). No diffraction signal associated with the graphite was observed indicating that the GO was fully oxidized and

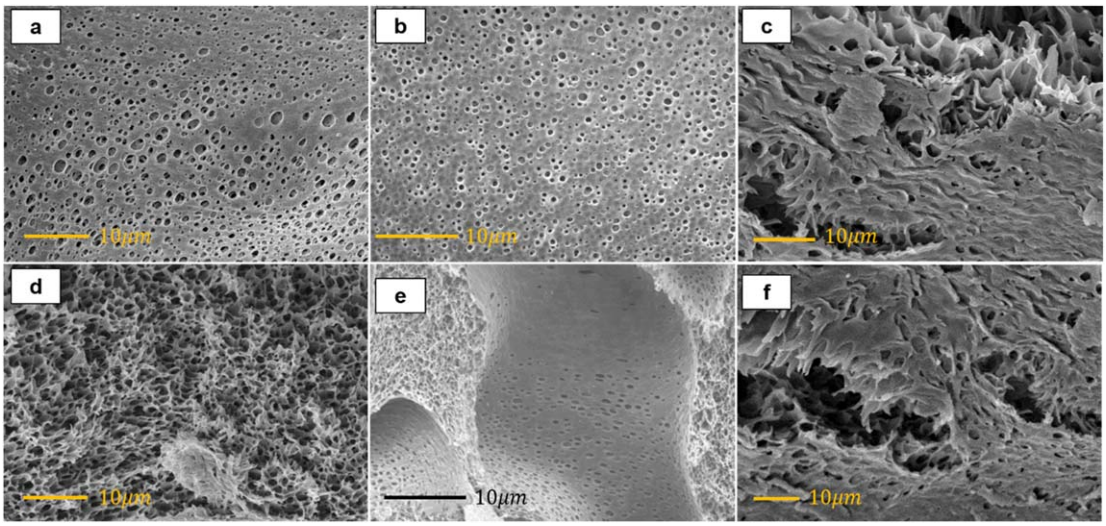


**Figure 4.** Surface morphology of the nanocomposite membranes (a) PPE2, (b) PPE4, (c) PPV2, (d) PEPVGO4, (e) PEPVGO2, and (f) PPV4.

does not contain any unoxidized graphite phase. After GO addition in PEPVGO2 and PEPVGO4, the diffraction peak (0 0 2) corresponding to the natural graphite was observed, stipulating that the GO layers were partially reduced after bonding with the polymeric matrix of the membrane identical peaks of GO, PEPVGO2, and PEPVGO4 at 10.8° demonstrate that these modified membrane materials contain a significant amount of GO phase (Gontarek-Castro *et al* 2021). However, the relatively large peak intensity of the GO phase in the PEPVGO2 and PEPVGO4 compared to the pure GO diffraction peak highlighted the increased crystallinity of the phases present in the membranes (Najafi *et al* 2017). The small peaks in PEPVGO2 and PEPVGO4 are due to the PES, PVP, and PEG. The PES diffraction peak was observed at 14.2° (Saedi *et al* 2014), and the signals at 18.3 and 21.67° are affiliated with the presence of PEG (Barron *et al* 2003) in the semi-crystalline polymeric matrix. On the other hand, the relatively small diffraction signals at 16.2 and 23.98° validated the presence of PVP (Zhang *et al* 2018). However, the major diffraction peak (at 10.8°) associated with the GO was evident in both PEPVGO2 and PEPVGO4 membrane samples, independent of the concentration of GO in these membrane samples.

### 3.3. Microscopic examination of the membrane samples

The microstructural features of the fabricated membrane samples after the addition of GO as nanofillers were examined by SEM analysis. The topographical features of the as-prepared composite membranes are shown in figure 4. These composite membranes were prepared by adding GO to the casting solution and surface functionality (as shown in the FTIR; figure 2(c)) of the GO ensured its compatibility and uniform dispersion in the polymeric solution thus avoiding its aggregation on the surface of the membranes. The cross-sectional images of the membrane samples highlighted the prominent effect of GO addition on the formation of porous structures (figure 5). In general, independent of the GO additions, all the PES membranes presented an asymmetric bi-layer porous structure containing a dense top layer and an underlying finger-like porous structure. Compared to the pristine PES membrane, the size of the pores in the PES/GO nanocomposite was found to be larger as depicted in figure 5. In other words, the formation of finger-like pore channels in the PES/GO membranes was found slightly broader than the pores developed in the pristine PES membrane. These features suggest that the hydrophilic character of GO could significantly boost the exchange rate between nonsolvent and solvent during a coagulation step and resulted in the development of relatively larger pore channels.

The cross-sectional microstructure of the pure PPE2, PPE4, PPV2, PPV4, PEPVGO2, and PEPVGO4 membrane samples are shown in figure 5. These cross-sectional images of the membrane samples indicated the active membrane top layer and underlying inhomogeneous porous structure corresponding to the non-woven polyethylene/polypropylene support. Membranes containing PVP were denser, having a top layer of a few tens of micrometres. This could be due to the high PES amount in the casting solution (19 wt% for 80 wt% of NMP), which becomes highly viscous and favored the generation of membranes with fewer macro voids in comparison to membranes manufactured from the casting solutions containing only PES. Pure PES-based membranes demonstrate a more asymmetrical morphology containing micro-voids of a few micrometres in length. Such membranes bear lower permeability compared to PES/PVP membranes possibly due to the hydrophilic nature

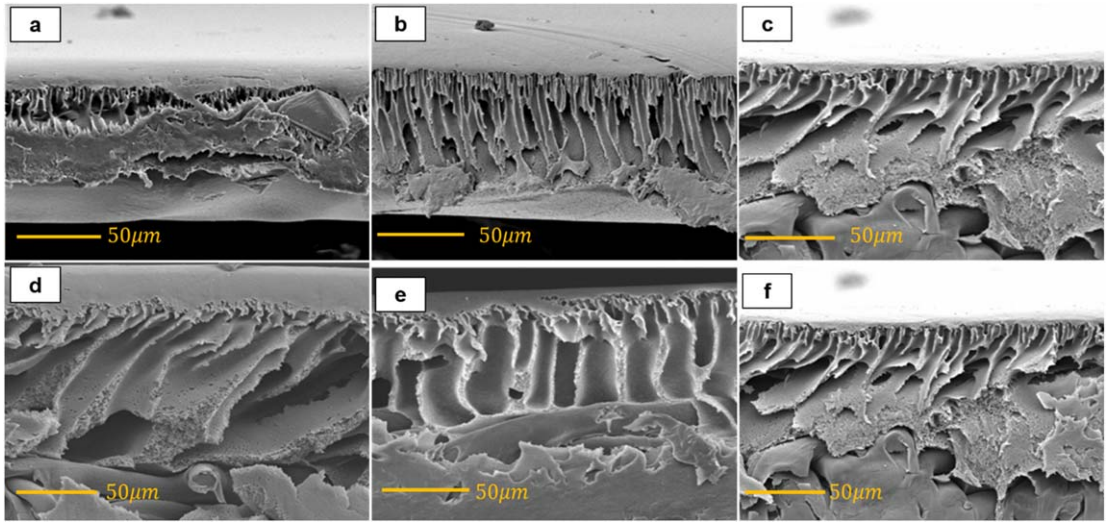


**Figure 5.** Cross-sectional images of the GO-PES membranes (a) PPE2, (b) PPE4, (c) PPV2, (d) PEPVGO4, (e) PEPVGO2, and (f) PPV4.

of the PVP. It is highlighted that by increasing the GO concentration from 0.2 to 0.4 wt%, the density of the pore (or simply the porosity) was increased appreciably as evident in figures 4 and 5. The pore blockage and agglomeration were observed in the PPEPVGO4 membrane sample, which is attributed to the presence of a high concentration of GO (0.4 wt%) in the matrix. The variation in membrane structure corresponded to the hydrophilic nature of the GO. The addition of a large amount of GO in the casting mixture increased the hydrophilicity of the membranes corresponding to the rapid exchange between the solvent/non-solvent (NMP) phases during the phase inversion step in the synthesis process. The addition of GO in the PES increases the porosity of the membranes due to the formation of large-size pores resulting in the generation of finger-like porous channels. The development of large size pores in the membrane could enhance the water flux and highlights the benefits of GO addition in the PES-based membranes.

### 3.4. Surface roughness, water uptake capacity and wettability of the membrane samples

The surface roughness is a highly efficacious parameter to estimate the fouling characteristics of the membranes. The optical profilometry analysis was carried out to measure the surface roughness of the membrane samples. The increase in the surface roughness was directly related to the concentration of GO in the membranes as shown in figure 6(a). According to the optical profilometry results, the increase in surface roughness of the membranes with the increase in the GO concentration was possibly associated with the hydrophilic nature of the GO that could migrate to the active layer of the membrane during the phase exchange process. In other words, it is suggested that during the phase inversion process, the migration of GO towards the surface of the membrane increased the surface roughness and hydrophilicity of the PEPVGO2 and PEPVGO4 membranes (Mahmoudi *et al* 2019a).

The hydrophilicity of the membrane significantly influences the antifouling characteristics of the membranes and is an important consideration in membrane design. The hydrophilicity is calculated by measuring the DI water contact angle on the membrane surface (Wen *et al* 2017). According to the obtained data shown in figure 6(b), a notable decline in the contact angle (or increase in the surface wettability) of the GO-containing nanocomposite membranes was observed. Due to its hydrophobic nature, the pristine membrane exhibited the highest contact angle (86.8°), while the PEPVGO4 sample having 0.4 wt% of GO concentration showed the lowest contact angle (28°). This appreciable decrease in contact angle confirmed the amplification in the surface hydrophilicity due to the addition of GO in the nanocomposite membranes. The increased surface hydrophilicity and finger-like porous surface morphology of the membrane were associated with the GO addition in the polymeric matrix (Mahmoudi *et al* 2019b) (Qian *et al* 2018). The hydrophilicity of the membrane samples i.e., PPE2, PPE4, PPV2, PPV4, PEPVGO2, and PEPVGO4, can be estimated from the contact angles values i.e., 61°, 59°, 48°, 45°, 34°, and 28°, respectively. The membrane sample, PEPVGO4 (GO/PEG/PVP/PES ratio is 1) presented a slightly low contact angle (large wettability) compared to PEPVGO2 (GO/PEG/PVP/PES ratio is 0.5), possibly associated with the large GO contents. During the non-solvent exchange and solvent phase inversion process, GO showed more affinity towards water (non-solvent) due to its hydrophilic nature and it moved towards the membrane surface (in the active surface layer) owing to the presence of water in the polymeric mixture during synthesis process (Bhatti *et al* 2018). The increase in the GO loading from 0.2 to

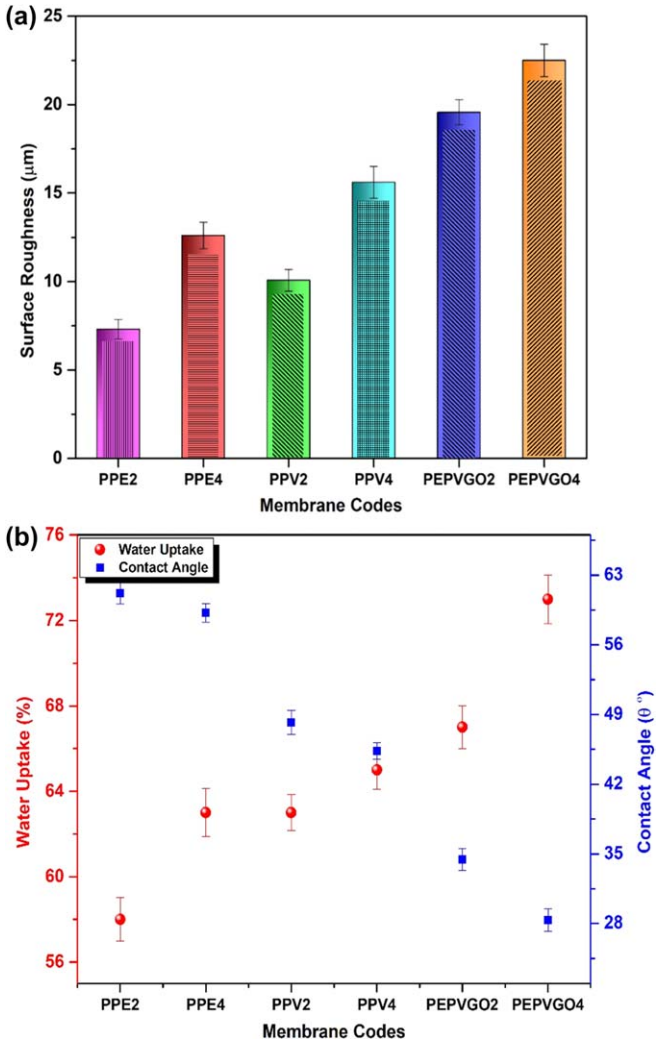


**Figure 6.** (a) The effect of additives on the surface roughness of the membrane samples (b) variation in contact angles and water uptake capacity of the membrane sample containing various amounts of organic additives and GO contents.

0.4 wt% resulted in the improvement in the surface wettability of the membranes and is highlighted by the appreciably large water uptake capacity of the membranes (from 66 to 73%). Further increase in GO loading $>$ 0.4 wt% could increase the contact angle possibly due to the agglomeration of GO in the membrane as suggested by (Wang *et al* 2018). Compared to the pristine PES membrane, which presented significantly low water uptake capacity (~58%), an appreciable decrease in the contact angle by the GO-loaded membranes samples validated their improved hydrophilic character (Yang *et al* 2019).

The pristine PES membrane shows minimum water retention capacity due to the hydrophobic property of the PES. Membrane samples loaded with GO (PEPVGO2, PEPVGO4) particles registered higher water retention capacity compared to the other membrane samples (without GO). For instance, PEPVGO4 registered the highest water retention capacity of 73%, as shown in figure 6(b). The improvement in the water retention capacity of the GO-containing membranes is associated with the increase in their hydrophilicity as indicated by the appreciably low contact angle (28°). However, no remarkable difference between PPE4, PPV2, and PPV4 was observed. It has been observed that a further increase in GO contents ($>$ 0.4 wt%) in the membrane samples could significantly promote the agglomeration of GO which reduced the hydrophilicity and water retention capacity (the results are not shown here).

### 3.5. Estimation of porosity, water flux and salt rejection capacity

As shown in figure 7(a), the % porosity values of the as-synthesized membranes ranged between 42 to 77%, which is attributed to the decrease in PES concentration in the membrane due to the increase in the PVP concentration. Due to the higher miscibility of PVP with water, its leaching from the membrane matrix is expected during the bath's solvent exchange and coagulation process. The preferential leaching of the PVP from the polymeric matrix could be associated with the finger-like porous structure as discussed above.

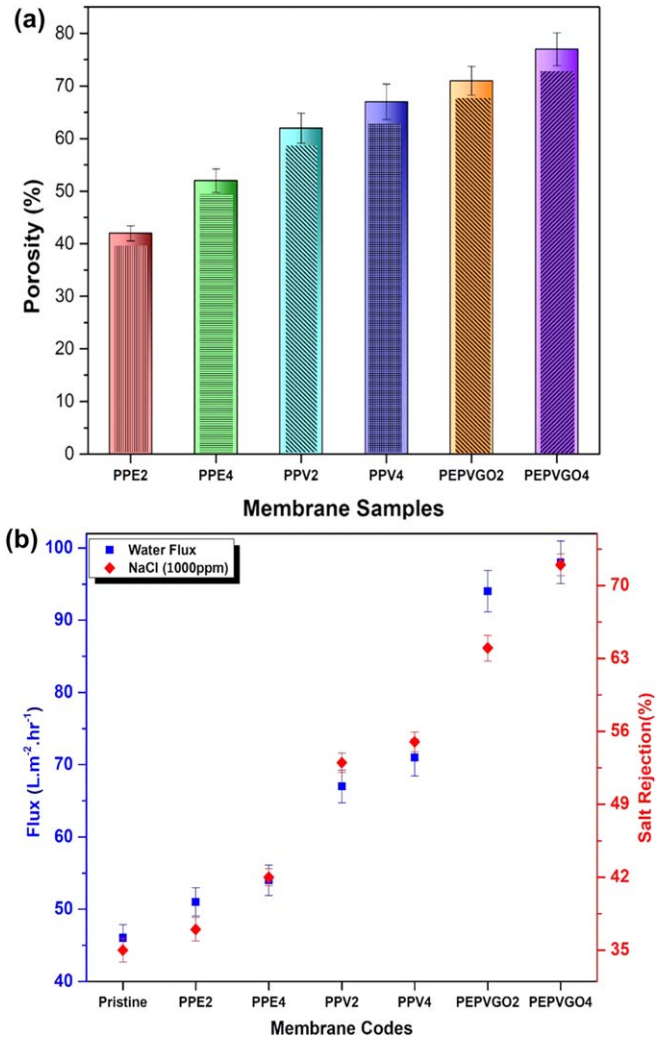


**Figure 7.** (a) Percent porosity of the pristine and modified membrane samples (**b**) Water flux and salt rejection capabilities of the as-synthesized membrane samples.

The synthesized membrane samples showed a larger pore volume in the sublayer than in the pristine PES membranes containing no PVP. However, the porosity of the PPV2 and PPV4 membrane was increased from 62 to 67%, with an increase in PVP concentration as shown in figure 7(a). Furthermore, the addition of GO induces a slight positive effect on the % porosity and a slightly large % porosity of approximately 71 and 77% was exhibited by the 0.2 and 0.4 wt% GO containing membrane samples, respectively. The aggregation of GO with high GO loading is a plausible explanation for such behavior. For instance, the hydrophilic character of the GO wettability could also affect the non-solvent/solvent exchange during the phase-inversion process thus resulting in improved membrane surface porosity and permeability. On the other hand, it was observed that with the increase in GO concentration $>$ 0.2 wt%, the viscosity of the casting mixture could increase and may result in the reduction of mean pore radius and membrane porosity.

The water permeation through the synthesized membrane samples was determined at 60 cm Hg of pressure. Increasing the GO contents in the fabricated membrane increased the water permeation flux as shown in figure 7(b). The pristine membrane (PPE2) sample registered the lowest flux value of ~52 l $m^{-2}h^{-1}$, which increased with the addition of PEG, PVP, and GO in the PEG $<$ PVP $<$ GO order. Compared to PEG, the addition of PVP significantly increase the water flux due to the increase in the membrane porosity. However, with the increase in PEG and PVP concentration (from 0.2 to 0.4 wt%) in the PPE2, PPE4 and PPV2, PPV4, membrane samples, respectively, a slight change in the water flux was observed. For instance, with an increase in PVP concentration in the PPV membrane samples (PPV2 and PPV4), there was a negligible effect on the water flux values (~68–70 l.$m^2$.$hr^{-1}$). On the other hand, compared to PPE and PPV membrane samples, PEPVG02 and PEPVGO4 offered the highest water flux, i.e., 94 and 96 l-$m^{-2}h^{-1}$, respectively owing to their large porosity. The lowest water flux of the pristine PES membrane (~45 l-$m^{-2}h^{-1}$) was due to its hydrophobic nature. Also, the PES membranes have unstructured finger-like channels and small pores in their architecture thus presenting the

**Table 2.** Comparison of the as-prepared membranes and other membranes reported in the literature. (*dye rejection)

| References | Concentration of additives (wt%) | Water flux ($l.m^{-2}.h^{-1}$) | Salt rejection (%) | Water contact angle (degree) |
|---|---|---|---|---|
| (Zinadini 2014) | PES + 1.0 PVP + 0.1 GO | 13.2 | 98* | 58.6 |
| | PES + 1.0 PVP + 0.5 GO | 20.4 | 96* | 53.2 |
| (Bhatti *et al* 2018) | PES + 0.0025 GO | 50 | 41 | 61 |
| | PES + 0.00625 GO | 142.1 | 60.1 | 53 |
| | PES + 0.0125 GO | 41.26 | 69.4 | 56 |
| (Karkooti *et al* 2018) | PES + 0.1 GO | 18 | — | 51.1 |
| (Yu *et al* 2013) | PES + 8 PVP + 0.8 Acetone + 72.2 DMAc + 1 HPEI-GO | 172 | — | ~77 |
| | PES + 8 PVP + 0.8 Acetone + 70.2 DMAc + 3 HPEI-GO | 165 | — | ~70 |
| | PES + 8 PVP + 0.8 Acetone + 68.2 DMAc + 5 HPEI-GO | 155 | — | ~65 |
| This work | PES + 0.2 PEG + 0.2 PVP + 0.2 GO | 90 | 64 | 34 |
| | PES + 0.4 PEG + 0.4 PVP + 0.4 GO | 95 | 72 | 28 |

lowest water flux. Further, with the addition of GO nanoparticles in the membrane samples, the large water flux values were associated with their well-defined porous structure and improved hydrophilic character. The beneficial effects of GO addition in the PES membranes are evaluated in terms of their improved hydrophilicity and water retention and flux capabilities (Wen *et al* 2017) (Gontarek-Castro *et al* 2021). The large diameter finger-like channels formed in the GO-containing membranes (PEPVGO2 and PEPVGO4) resulted in an appreciable improvement in the water flux as evident in figure 7(b).

Akin to water flux, a similar trend of the membrane samples in terms of salt rejection was observed as shown in figure 7(b). The increase in salt rejection was observed and the tendency followed the order of PPE2 <PPE4 <PPV2 <PPV4 <PEPVGO2 <PEPVGO4. This implies that the membrane samples containing a large amount of GO as nanofillers exhibited a higher nanofiltration tendency (salt rejection > 70%). Compared to PPE2 and PPE4, the % salt rejection by the PEPVGO2 (64%) and PEPVGO4 (72%) membrane samples was approximately two times larger in magnitude. This range of salt rejection is not very impressive but for ultra-filtration membranes, this range is quite acceptable.

The overall performance of the as-synthesized GO-PES membranes is also compared with the other membranes reported in the literature. The water flux, salt rejection capability, and contact angle values are summarized in table 2. In comparison, acceptable water flux, % salt rejection and significantly improved wettability of the 0.2 and 0.4% GO-containing membranes highlighted their potential applicability on a commercial scale. Also, the primary interest of this work was to improve the wettability and anti-fouling characteristics (as discussed below) of the membranes without compromising the water flux and salt rejection capabilities. As evident from the results, these membranes could be applied where anti-fouling properties are of prime importance than salt-rejection.

### 3.6. Antibacterial activity of the membranes

The disk diffusion method was used to calculate the diameter of the inhibition zone (DIZ) of *E. coli* and *S. aureus* bacterial strains on the surface of GO and GO-PES composite membranes. Bacteria-infested water was used to test the antibacterial activity of GO and composite suspensions in aquatic media. The survival frequency plate counting method was examined after 48 h of incubation under continuous shaking. The growth of bacteria in the controlled medium has been used as a reference for comparison and other membrane samples with and without GO were exposed to the bacterial suspension. The bacterial strains prone to lysis or larger cell death show greater DIZ, however, resistant strains could be sustained in the aggressive media and present small DIZ. After 48 h of incubation, a tiny inhibition zone was discovered surrounding the GO-containing membrane disk sample, representing sufficient inhibition in bacterial proliferation. In comparison, the disks having GO-PES nanoparticles were surrounded by a vibrant and remarkably larger DIZ for both *S. aureus* and *E. coli*. Compared to pristine PES, the average DIZ value of the GO-containing membrane samples was significantly large as shown in figure 8. An appreciable increase in the antibacterial activity of the *E. coli* bacterial strain (from 56.9% to 98.0% for PEPVGO2 and PEPVGO4, respectively) indicated the improvement in the anti-fouling characteristics of the membranes owing to the increase in the GO concentration from 0.2 to 0.4 wt%. In other words, the PES membranes blended with GO presented significantly large antibacterial activity, as indicated in figure 8. The antibacterial properties of the GO-containing membrane samples were associated with the hydrophilic nature of the membranes. The presence of active functional moieties in the polymeric matrix and the hydrophilic nature

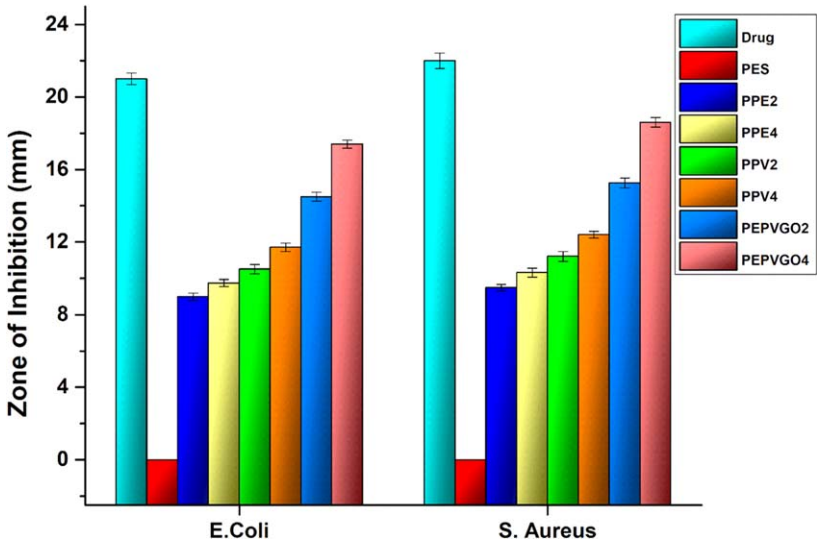


**Figure 8.** Antibacterial activity of the membrane samples presented as the spread of the inhibition zone.

of the GO produced an oxidizing condition at the surface of membrane samples resulting in bacteria death, owing to the progress of cell lysis. The decrease in the cell viability and death of the bacteria due to the presence of GO on the membrane surface has also been discussed by (Malaisamy *et al* 2010). Membranes loaded with GO also depicted a significant increase in the DIZ in the case of *S. aureus)* bacteria indicating the formation of non-tolerant surface for bacteria survival. The increased inhibition in the bacterial cell proliferation was exhibited by the PPEPVGO4 membrane sample. These results deduce that compared to the pristine PES membranes, the GO-loaded membranes presented notable antibacterial characteristics toward *S. aureus* and *E. coli* bacterial strains as exhibited by the histograms (figure 8).

The 62.3% and 89.8% DIZ values were calculated for *S. aureus* in contact with PEPVGO2 and PEPVGO4 disk samples, respectively indicating a more robust resistance against *E. coli* than *S. aureus* strains. The formation of a peptidoglycan layer was the more distinctive feature of the Gram-positive and Gram-negative bacteria. A relatively thick peptidoglycan layer (~ 20–80 nm) was formed by the Gram-positive bacteria compared to Gram-negative (7–8 nm). The presence of this thick layer in *S. aureus* hindered the ingress of the silver nanoparticles from the solution to the membrane surface, which controlled the antimicrobial activity. This behavior was associated with the variation in porosity and structure of the membranes, which was developed by the addition of various additives during their synthesis.

## 4. Conclusions

In this study, the preparation of PES-GO nanocomposite membranes via the phase inversion method is reported. The FT-IR results validated the presence of carboxylic acid, hydroxyl, and epoxy ring functional groups on the top surface of PES-GO membranes. The addition of GO in the PES significantly increased the porosity, hydrophilicity, water retention, flux, and salt rejection capabilities of the membranes. The addition of 0.4% wt of GO in the PEPVGO4 composite membrane shows an appreciably low contact angle (28°) highlighting the improved hydrophilicity of this membrane. A significant increase in the water flux of 96 lit-$m^{-2}$ $h^{-1}$ compared to the pristine PES membrane (43 lit $m^{-2}$-$h^{-1}$) was also registered by this membrane. In addition, the increase in salt rejection capability from 36% (pristine PES membrane) to 72% with improved antibacterial activity was exhibited by the PEPVGO4 composite membrane. Appreciably large wettability and antibacterial properties, effectiveness and long-term durability against Gram-negative *E. coli* and Gram-positive *S. aureus* also suggest that these novel PES-GO nanocomposite membranes hold effective prospects in industrial applications.

## Acknowledgments

The authors are thankful to the National University of Sciences and Technology (NUST) Research Directorate, HEC and NRPU through Project No. 6020 for all the technical assistance and financial support.

## Data availability statement

All data that support the findings of this study are included within the article (and any supplementary files). Further information can be obtained from the author(s) with a reasonable request.

## Conflict of interest

The authors declare no conflict of interest.

## ORCID iDs

Muhammad Asad Abbas https://orcid.org/0000-0003-4727-7958
Muhammad Yasir https://orcid.org/0000-0001-8999-2779
Kashif Mairaj Deen https://orcid.org/0000-0002-3619-2599

## References

Abbas M A *et al* 2020 Surface modification of TFC-PA RO membrane by grafting hydrophilic ph switchable poly(acrylic acid) brushes *Adv. Polym. Technol.* **2020** 8281058
Aditya Kiran S, Lukka Thuyavan Y, Arthanareeswaran G, Matsuura T and Ismail A F 2016 Impact of graphene oxide embedded polyethersulfone membranes for the effective treatment of distillery effluent *Chem. Eng. J.* **286** 528–37
Alammar A, Park S H, Williams C J, Derby B and Szekely G 2020 Oil-in-water separation with graphene-based nanocomposite membranes for produced water treatment *In Journal of Membrane Science* **603** 118007
Arif Z, Sethy N K, Kumari L, Mishra P K and Verma B 2019 Antifouling behavior of PVDF/$TiO_2$ composite membrane: a quantitative and qualitative assessment *Iran. Polym. J. (English Ed.)* **28** 301–12
Barron M K, Young T J, Johnston K P and Williams R O 2003 Investigation of processing parameters of spray freezing into the la liquid to prepare polyethylene glycol polymeric particles for drug delivery *AAPS Pharm Sci. Tech.* **4** 1–13
Batool M, Shafeeq A, Haider B and Ahmad N M 2021 $TiO_2$ nanoparticle filler-based mixed-matrix pes/ca nanofiltration membranes for enhanced desalination *Membranes (Basel).* **11** 433
Bhatti H T *et al* 2018 Graphene oxide-pes-based mixed matrix membranes for controllable antibacterial activity against salmonella typhi and water treatment *In International Journal of Polymer Science* **2018** 1–12
Boretti A and Rosa L 2019 Reassessing the projections of the world water development report *npj Clean Water* **2** 15
Chou W-L, Yu D-G and Yang M-C 2005 The preparation and characterization of silver-loading cellulose acetate hollow fiber membrane for water treatment *Polym. Adv. Technol.* **16** 600–7
Choudhury R R, Gohil J M, Mohanty S and Nayak S K 2018 Antifouling, fouling release, and antimicrobial materials for surface modification of reverse osmosis and nanofiltration membranes *J. Mater. Chem. A* **6** 313–33
Du J R, Peldszus S, Huck P M and Feng X 2009 Modification of poly(vinylidene fluoride) ultrafiltration membranes with poly(vinyl alcohol) for fouling control in drinking water treatment *Water Res.* **43** 4559–68
Li Q and Elimelech M 2004 organic fouling and chemical cleaning of nanofiltration membranes: Measurements and Mechanisms *Environ. Sci. Technol.* **38** 4683–93
Esfahani M R *et al* 2019 Nanocomposite membranes for water separation and purification: Fabrication, modification, and applications *Sep. Purif. Technol.* **213** 465–99
Goh P S, Wong K C and Ismail A F 2020 Nanocomposite membranes for liquid and gas separations from the perspective of nanostructure dimensions *Membranes (Basel).* **10** 1–29
Gontarek-Castro E, Rybarczyk M K, Castro-Muñoz R, Morales-Jiménez M, Barragán-Huerta B and Lieder M 2021 Characterization of PVDF/graphene nanocomposite membranes for water desalination with enhanced antifungal activity *Water (Switzerland)* **13** 1279
Guo H, Chen P, Tian S, Ma Y, Li Q, Wen C, Yang J and Zhang L 2020 Amphiphilic marine antifouling coatings based on hydrophilic polyvinylpyrrolidone and a hydrophobic fluorine-silicon-containing block copolymer *Langmuir* **36** 14573–81
Jeon S, Rajabzadeh S, Okamura R, Ishigami T, Hasegawa S, Kato N and Matsuyama H 2016 The effect of membrane material and surface pore size on the fouling properties of submerged membranes *Water (Switzerland)* **8** 602
Ji Y, Qian W, Yu Y, An Q, Liu L, Zhou Y and Gao C 2017 Recent developments in nanofiltration membranes based on nanomaterials *Chinese J. Chem. Eng.* **25** 1639–52
Karkooti A, Yazdi A Z, Chen P, McGregor M, Nazemifard N and Sadrzadeh M 2018 Development of advanced nanocomposite membranes using graphene nanoribbons and nanosheets for water treatment *In Journal of Membrane Science* **560** 97–107
Kim H J, Choi K, Baek Y, Kim D G, Shim J, Yoon J and Lee J C 2014 High-performance reverse osmosis CNT/polyamide nanocomposite membrane by controlled interfacial interactions *ACS Appl. Mater. Interfaces* **6** 2819–29
Lu le T, Dung N T, Tung le D, Thanh C T, Quy O K, Chuc N V, Maenosono S and Thanh N T 2015 Synthesis of magnetic cobalt ferrite nanoparticles with controlled morphology, monodispersity,y, and composition: the influence of solvent, surfactant, reductant, and synthetic conditions *Nanoscale* **7** 19596–610
Mahmoudi E, Ng L Y, Ang W L, Chung Y T, Rohani R and Mohammad A W 2019a enhancing morphology and separation performance of polyamide 6, 6 membranes by minimal incorporation of silver decorated graphene oxide nanoparticles *Sci Rep.* **9** 1–16
Mahmoudi E, Ng L Y, Ang W L, Chung Y T, Rohani R and Mohammad A W 2019b Enhancing morphology and separation performance of polyamide 6, 6 membranes by minimal incorporation of silver decorated graphene oxide nanoparticles *Sci Rep.* **9** 1216
Malaisamy R, Berry D, Holder D, Raskin L, Lepak L and Jones K L 2010 Development of reactive thin film polymer brush membranes to prevent biofouling *J. Memb. Sci.* **350** 361–70
Mansouri J, Harrisson S and Chen V 2010 Strategies for controlling biofouling in membrane filtration systems: challenges and opportunities *J. Mater. Chem.* **20** 4567–86

Najafi M, Kermanpur A, Rahimipour M R and Najafizadeh A 2017 Effect of $TiO_2$ morphology on the structure of $TiO_2$-graphene oxide nanocomposite synthesized via a one-step hydrothermal method *J. Alloys Compd.* **722** 272–7
Ngo T H A, Nguyen D T, Do K D, Minh Nguyen T T, Mori S and Tran D T 2016 Surface modification of polyamide thin film composite membrane by a coating of titanium dioxide nanoparticles *J. Sci. Adv. Mater. Devices* **1** 468–75
Park J A, Cho K Y, Han C H, Nam A, Kim J H, Lee S H and Choi J W 2019 Quaternized amphiphilic block copolymers/graphene oxide and a poly(vinyl alcohol) coating layer on graphene oxide/poly(vinylidene fluoride) electrospun nanofibers for superhydrophilic and antibacterial properties *Sci Rep.* **9** 1–13
Qadir D, Mukhtar H and Keong L K 2017 Mixed matrix membranes for water purification applications *Sep. Purif. Rev.* **46** 62–80
Qian X, Li N, Wang Q and Ji S 2018 Chitosan/graphene oxide mixed matrix membrane with enhanced water permeability for high-salinity water desalination by pervaporation *Desalination* **438** 83–96
Rana D and Matsuura T 2010 *Surface Modifications for Antifouling Membranes* **110** 2448–71
Saedi S, Madaeni S S, Hassanzadeh K, Shamsabadi A A and Laki S 2014 The effect of polyurethane on the structure and performance of PES membrane for separation of carbon dioxide from methane *J. Ind. Eng. Chem.* **20** 1916–29
Said N N, Hamzah F, Ramlee N A and Yunus N N 2018 The effect of $TiO_2$ particles addition on the characteristics of polysulfone membrane *Int. J. Adv. Sci. Eng. Inf. Technol.* **8** 825–31
Shahkaramipour N, Tran T N, Ramanan S and Lin H 2017 Membranes with surface-enhanced antifouling properties for water purification *Membranes (Basel).* **7** 1–18
Ulbricht M 2006 Advanced functional polymer membranes *Polymer* **47** 2217–62
Wang X, Feng M, Liu Y, Deng H and Lu J 2019 Fabrication of graphene oxide blended polyethersulfone membranes via phase inversion assisted by electric field for improved separation and antifouling performance *In Journal of Membrane Science* **577** 41–50
Wang Y, Lu Y, Zhang J, Hu X, Yang Z, Guo Y and Wang Y 2019 A synergistic antibacterial effect between terbium ions and reduced graphene oxide in a poly(vinyl alcohol)-alginate hydrogel for treating infected chronic wounds *Journal of Materials Chemistry B* **7** 538–47
Wen P, Chen Y, Hu X, Cheng B, Liu D, Zhang Y and Nair S 2017 Polyathin-film film composite nanofiltration membrane modified with acyl chlorided graphene oxide *J. Memb. Sci.* **535** 208–20
Yang Z, Zhou Y, Feng Z, Rui X, Zhang T and Zhang Z 2019 A review on reverse osmosis and nanofiltration membranes for water purification *Polymers (Basel).* **11** 1–22
Yin J and Deng B 2015 Polymer-matrix nanocomposite membranes for water treatment *J. Memb. Sci.* **479** 256–75
Ying Y, Ying W, Li Q, Meng D, Ren G, Yan R and Peng X 2017 Recent advances of nanomaterial-based membrane for water purification *Appl. Mater. Today* **7** 144–58
Yu L, Zhang Y, Zhang B, Liu J, Zhang H and Song C 2013 Preparation and characterization of HPEI-GO/PES ultrafiltration membrane with antifouling and antibacterial properties *In Journal of Membrane Science* **447** 452–62
Zhang J, Yuan B and Ren H 2018 Synthesis and characterization of PVP/$Tb_{4/3}$L·$7H_2O$ luminescent complex *IOP Conf. Series: Earth and Environmental Science (Online)* **170** 6
Zhao C, Xue J, Ran F and Sun S 2013 Modification of polyethersulfone membranes - a review of methods *Prog. Mater Sci.* **58** 76–150
Zinadini S, Zinatizadeh A A, Rahimi M, Vatanpour V and Zangeneh H 2014 Preparation of a novel antifouling mixed matrix PES membrane by embedding graphene oxide nanoplates *J. Mem. Sci.* **453** 292–301